Spatially-Resolved Mapping of 3D Molecular Orientations with ~2 nm Spatial Resolution through Tip-Enhanced Raman Scattering

Patrick Z. El-Khoury,[1,] Edoardo Aprà[2]*

[1]Physical Sciences Division, [2]Environmental Molecular Sciences Laboratory, Pacific Northwest National Laboratory; P.O. Box 999, Richland, WA 99352, USA

*patrick.elkhoury@pnnl.gov

ABSTRACT

We record local optical field images of silver nanocubes (75 nm) using tip-enhanced Raman (TER) spectral imaging. The images we observe are consistent with several recent reports from our group, but here, we demonstrate sub-2 nm spatial resolution in local optical field nano-imaging under ambient laboratory conditions. This is achieved by scanning the substrate (nanocube on Si) relative to a 4-thiobenzonitrile (TBN)-functionalized Ag-coated TER probe. The spatial resolution we obtain necessitates that only a few molecules govern the recorded optical response; molecular orientation becomes an important consideration in such measurements. We model the orientation through geometry optimization of a TBN molecule chemisorbed onto an Ag_{79} cluster (sphere with a ~1 nm diameter). Using the computed orientation of the cluster-bound molecule, we then model the optical response using a formalism that accounts for the orientation of the molecule relative to vector components of the local optical fields. We find optimal agreement between experiment and theory. In effect, this work reveals the parallels between single molecule Raman scattering and high-spatial resolution TER spectroscopy, even when the images themselves cannot be used to visualize a single molecule in real space.

Introduction

Tip-enhanced Raman (TER) nano-imaging and nano-spectroscopy combine the unique properties of scanning probe (herein atomic force) microscopy and Raman scattering.[1-3] This technique is rooted in surface-enhanced Raman (SER) spectroscopy,[4-7] where combinations of electromagnetic and chemical enhancement significantly boost the detection limits of Raman scattering.[3] One of the distinct advantages of TER over SER is the former technique's ability to resolve the enhanced optical response over the nanometer length scale by scanning the sample relative to a laser-irradiated plasmonic probe. Recent works have demonstrated Raman mapping with sub-molecular resolution using TER spectral imaging.[8-11] Although the attainable spatial resolution in low temperature/ultra-high vacuum TER is now established, the same cannot be said of measurements performed under ambient laboratory conditions. Namely, there is a dichotomy between decades of TER reports that claim tip radius-limited spatial resolution (10s of nm) and more recent investigations, whereby single/few nm spatial resolution in ambient TER nano-imaging has been observed.[12] Nanoscale chemical mapping of single-stranded DNA with single base resolution is one elegant demonstration that comes to mind in the context of the latter.[8]

Through TER mapping of plasmonic nanostructures and nanoparticles, our group has repeatedly demonstrated ~3-5 nm spatial resolution in chemical nano-images recorded under ambient laboratory conditions.[13-16] Our initial studies focused on establishing that TER maps of plasmonic particles trace the profiles of local optical fields in their immediate vicinities.[14-19] For instance, TER maps of plasmonic Au nanorods traced both dipolar and multipolar resonances that are characteristic of such particles.[20] In our case of TER nano-imaging of plasmonic nanostructures and nanoparticles, the attainable spatial resolution seems to be limited by the

structures of the local optical fields in the gap mode TERS configuration.[14, 21] Namely, gentle local optical field variations in space yield lower (apparent) spatial resolutions in TER mapping. In this regard, the highest measured spatial resolution in local optical field mapping we have demonstrated takes advantage of spatially confined hybrid plasmonic probe-silver nanoparticle nanojunctions.[14] For a detailed discussion of combined atomic force-TER mapping of the latter constructs, we refer the reader to our prior work.[14]

In all our former studies and current report, we employ nano-corrugated/sputtered Au (or Ag) plasmonic probes with large nominal tip radii (75-100 nm). We can rationalize our attainable resolution by recognizing that although the measured far-field resonances and optical field enhancements arise from the gross microscopic makeup of the tip, fine nanometer-scale features that are sustained at the tip apex govern the attainable spatial resolution.[12, 22] The same features seem to support unique local resonances that can be only (indirectly) observed via TER spectral imaging.[17, 22] Unfortunately, and although optical resonances that vary over the nanometer length scale may hold the key to rationalizing many fundamental observations in TER nano-imaging and nano-spectroscopy, they remain difficult to independently gauge in practice through, e.g., broad band extinction nano-spectroscopy experiments in the TER geometry.

In this work, we take advantage of a well characterized TER construct, namely, a plasmonic silver nano-cube which we image using a chemically functionalized Ag atomic force microscopy (AFM) probe irradiated at 633 nm. After demonstrating high spatial resolution in nano-imaging (sub-2 nm), we strive to rigorously establish the orientation of the tip-bound molecule(s), with a premise that the tensorial nature of TER scattering is a direct consequence of the ultra-confined probing volume. Unlike prior work, where full spatio-spectral TER spectral image fitting or full searches in Euler space were performed to either gauge molecular

orientation or the vector components of local electric field through TER/SER scattering, we now describe a preliminary step that can be used to narrow the search. Namely, we first establish molecular orientation of the tip bound molecules through geometry optimization of a model that consists of a 4-thiobenzonitrile (TBN) molecule chemisorbed onto a spherical silver nano-cluster (Ag_{79}). The size of the cluster (~1 nm) is commensurate with the measured spatial resolution in this study (down to 1.6 nm); we therefore propose that the cluster is representative of the tip apex. Confidence in our model is further obtained by obtaining successful spectral matches between experimental and simulated Raman spectra that account for the relative orientation between the molecule and the dominant local electric field direction in practice (along the tip axis). The models and theoretical framework we describe should be helpful in on-going efforts aimed at (i) imaging the vector components of local optical fields with computed/experimentally derived molecular orientations, and at (ii) imaging chemical transformations in real space through TER nano-imaging, as molecular orientations were found to play an important role in interfacial plasmon-enhanced/induced chemical transformations.[23]

Methods

Theoretical. We have used a development version of NWChem for all the calculations reported here.[24] Unconstrained geometry optimization of the Ag_{79}-TBN complex was performed using the PBE exchange-correlation functional[25] in conjunction with the def2-SVP basis[26] set and a fitting basis[27] for the evaluation of the Coulomb potential. The use of dispersion[28] did not affect the optimized geometrical parameters, as evident through an inspection of the overlaid structures (with/without dispersion correction) in Figure 1. In the optimized Ag_{79}-TBN complex, the aromatic ring of TBN is nearly parallel to the surface of the nanocluster; the molecule is otherwise at a small angle (~11^o) with respect to the surface. Geometry optimization and Raman

spectral simulations (*vide infra*) of the bare TBN molecule were performed using the PBE exchange-correlation functional[25] in conjunction with the Sadlej-PVTZ basis set.[29]

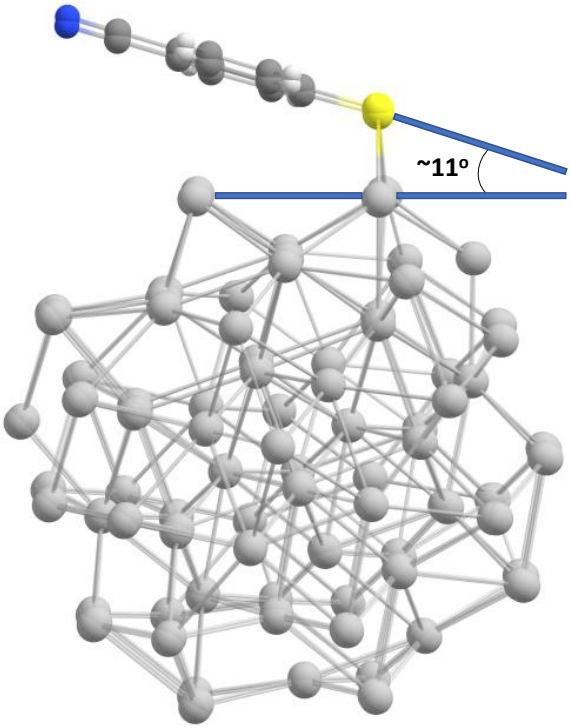

Figure 1. Overlaid molecular structures optimized with/without the inclusion of empirical dispersion. See text for more details.

Conventional ensemble-averaged Raman spectra and normal mode-dependent molecular polarizability derivatives were computed using the CPKS method, as implemented in NWChem.[24] Ensemble-averaged Raman scattering activities (S_m) are given by[30, 31]

$$S_m = g_m[45\alpha'_m{}^2 + 7\beta'_m{}^2] \quad (1)$$

where

$$\alpha'_m = \frac{1}{3}(\widetilde{\alpha}'_{xx,m} + \widetilde{\alpha}'_{yy,m} + \widetilde{\alpha}'_{zz,m}) \quad (2)$$

and

$$\beta'_m{}^2 = \frac{1}{2}[(\tilde{\alpha}'_{xx,m} - \tilde{\alpha}'_{yy,m})^2 + (\tilde{\alpha}'_{yy,m} - \tilde{\alpha}'_{zz,m})^2 + (\tilde{\alpha}'_{zz,m} - \tilde{\alpha}'_{xx,m})^2 + 6(\tilde{\alpha}'_{xy,m}{}^2 + \tilde{\alpha}'_{xz,m}{}^2 + \tilde{\alpha}'_{yz,m}{}^2)] \quad (3)$$

In the above equations, g_m is the vibrational state degeneracy and the primes correspond to derivatives with respect to the m^{th} state, $\alpha'_m//\beta'_m{}^2$ are the isotropic//anisotropic polarizabilies, and $\tilde{\alpha}'_{ij,m}$ (i,j = x,y,z) are individual components of the polarizability tensor. Experimental and calculated ensemble-averaged Raman spectra of TBN (see below) are shown in Figure 2. Since our ensuing analysis relies on the relative intensities of the observable vibrational states, we note the agreement between experiment and theory in the high-frequency (1400-2300 cm^{-1}) region of the spectrum that contains the aromatic CC stretching (~1589 cm-1) and CN stretching (2225 cm^{-1}) vibrations of TBN. The same cannot be said of the lower frequency modes in the 1000-1250 cm^{-1} spectral region.

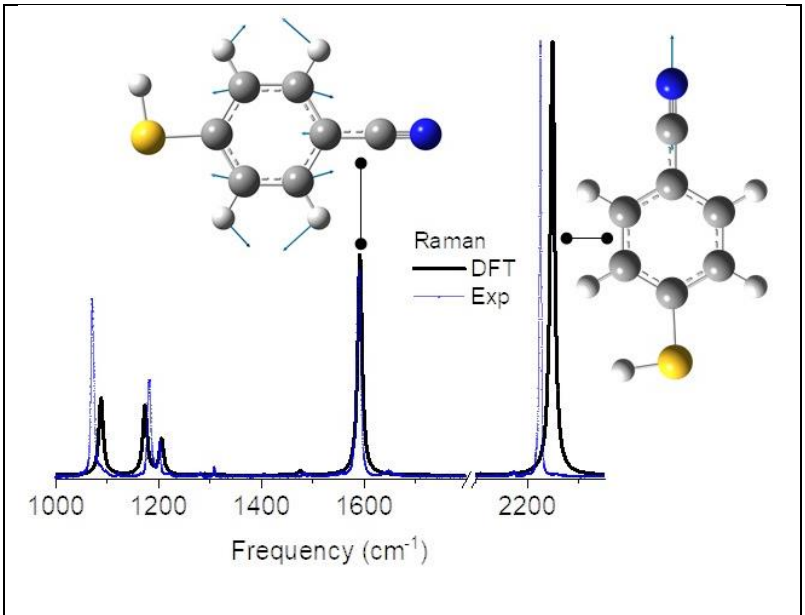

Figure 2. Experimental (TBN powder, blue) and computed (isolated molecule, black) ensemble-averaged Raman spectra. The inset shows a vector representation of the aromatic CC and CN stretching vibrations.

The spectrum of an oriented TBN molecule is simulated according to[16, 32]

$$S_n^2 \; \alpha \; \sum_n \left| \overrightarrow{E_s^L} R_z^T R_y^T R_x^T \widetilde{\alpha_n'} R_z R_y R_x \overrightarrow{E_i^L} \right|^2 \qquad (4)$$

in which molecular polarizability derivative tensor elements ($\widetilde{\alpha_n'}$) of the bare molecule (not linked to Ag_{79}) are oriented with respect to the vector components of the local electric field along incidence and scattering directions in the TER geometry ($\overrightarrow{E_{i,s}^L} = \overrightarrow{E_z^L}$) after (i) projection of the molecular onto the laboratory frame, and (ii) rotating the molecule (using rotation matrices $R_{x,y,z}$ and $R_{x,y,z}^T$) to match the computed orientation of TBN on Ag_{79} in the laboratory frame, see Figure 1. We will revisit this analysis in the ensuing sections of this work.

Experimental. Bulk Raman spectra of TBN (powder, Aurum Pharmatech) were recorded using an inverted optical microscope (Nikon Ti-E) coupled to a Raman spectrometer (LabRam HR, Horiba). Spectra were recorded using low power (10 μW) from a 633 nm laser source, which was focused onto the TBN crystals using a 60X (NA=0.7) air objective.

A 10 μL stock solution of 75 nm silver nanocubes (Sigma-Aldrich) was deposited onto a silicon chip. After the drop was air dried, the substrate was rinsed with excess amounts of ethanol. On a separate chip, we drop-casted 10 μL of a 1 mM ethanolic solution of TBN. The metal-coated AFM probe was functionalized simply by bringing the tip into contact with the TBN-coated substrate. The same method was previously used to functionalize TER probes with aromatic thiols.[16, 17]

Our TER setup is described elsewhere in detail.[13, 18, 22, 33] For the purpose of this work, as-purchased silicon probes (Nanosensors, ATEC) were coated with 100 nm of Ag and used for

AFM (tapping mode feedback) and TER (intermittent contact feedback) topographic/chemical imaging. For the latter, TER signals are collected when the tip is in direct contact with the surface. A semi-contact mode is otherwise used to move the sample relative to the tip (pixel to pixel). For TER measurements, a 633 nm laser (~75 μW) is focused onto the tip apex at a ~65^{o} angle with respect to the surface normal using a 100 X air objective (Mitutoyo, 0.7 NA). The polarization of the laser was set to coincide with the tip axis using a half-waveplate. The back-scattered light was collected using the same objective, filtered through a series of long pass/dichroic filters, and recorded using a CCD camera (Andor, Newton EMCCD) coupled to a spectrometer (Andor, Shamrock 500) equipped with a 300 l/mm grating blazed at 550 nm.

Results and Discussion

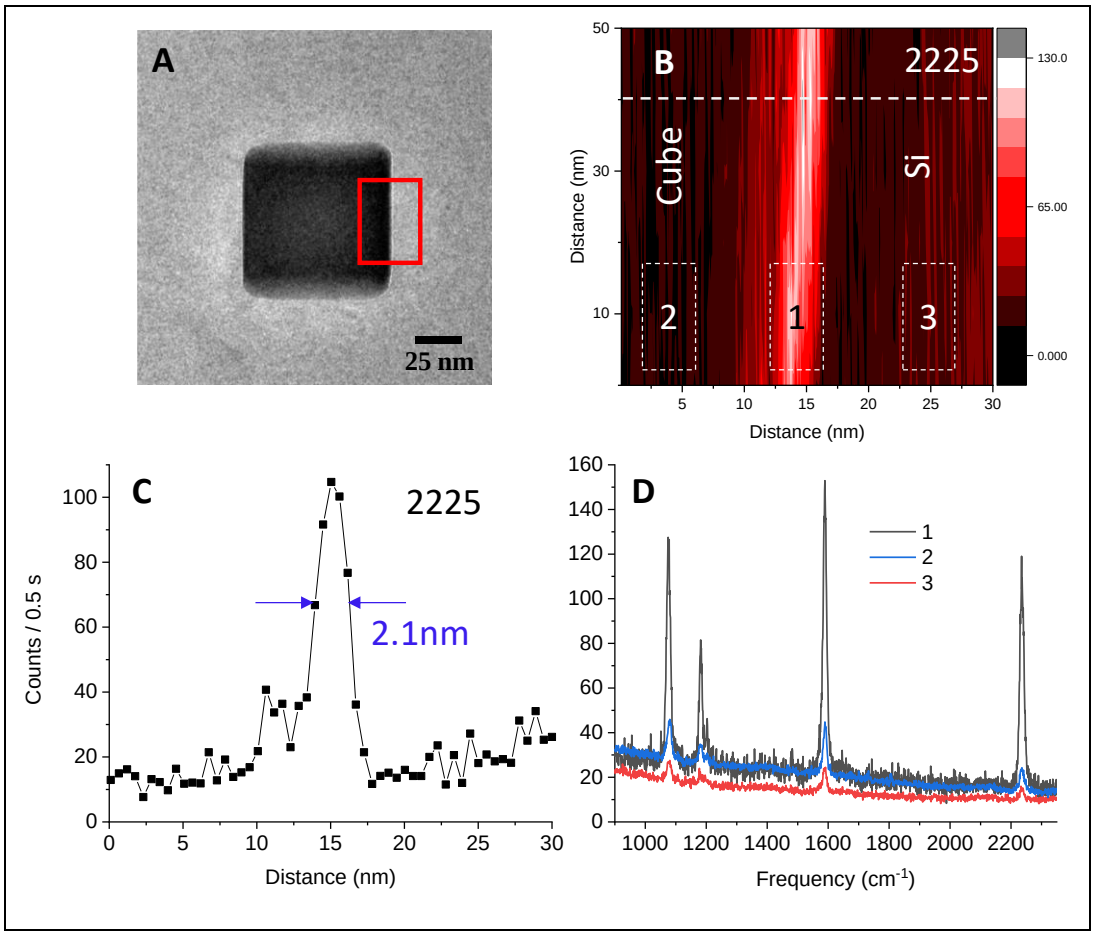

Figure 3. A representative TEM image of the nanocubes used herein is shown in panel A. The red rectangle highlights the region analyzed *via* nano-Raman spectral imaging. Panel B shows a ~2225 cm^{-1} TER image centered towards the edge of the cube (region 1). The same images traces the optical response when the tip is positioned on top of the cube (region 2) and on silicon (region 3). A TER cross-section (dashed horizontal line in panel B) that reveals the confinement of the optical response is plotted in panel C. Spatially averaged spectra contained in regions 1-3 are highlighted (dashed rectangles) in panel B and in turn compared on the same plot in panel D. The optical response was time-integrated for 0.5 s at each pixel, and the lateral step sizes were 0.5/10 nm along the horizontal/vertical directions.

The general topographic features of the silver nanocubes used in this work were described in detail in prior AFM-TER measurements from our group.[14] For the purpose of this work, a representative TEM image is shown in Figure 3A. TER images centered towards the edge of the cube (Figure 3B) are reminiscent of previously recorded TER maps of plasmonic nanostructures, including silver and gold nanocubes.[14, 33] Namely, the response towards the edge is significantly enhanced. As amply demonstrated in our prior reports,[14-16, 33] the recorded image traces local optical fields that vary in space when the nanocube is scanned relative to the plasmonic TER probe. [14, 33] The confined nature of the edge response (herein to ~2 nm, Figure 3C) provides a nanoscopic window for chemical and chemical reaction imaging.[21] Herein, the recorded spectra exhibit four dominant Raman-allowed resonances that can all be assigned to TBN based on our current (Figure 2) and prior theoretical analyses of this molecular reporter.[34, 35] We refrain from duplicating our prior analysis and refer the reader to previous work from our group for spectral assignments. Besides the structure of the local optical field as broadcasted through TER nano-imaging and the vibrational signatures of TBN that are recognizable from the spectra, several aspects of the TER image (Figure 3B) are worth noting. First, the reproducibility of the measurements (the attainable spatial resolution in particular) is ensured by virtue of the redundant nature of the construct (along the vertical direction). Namely, every horizontal trace across the edge yields a similar spatio-spectral profile (see Figures 3 and 4). As such, sample/tip

drifting and instabilities that are common under ambient conditions do not significantly contribute to the data within the time required to record these images (75s in the case of Figure 3B and 4). Second, the images are internally referenced. On-edge (region 1), on-particle (region 2) and off-particle/on-silicon (region 3) spectra are all contained within the same hyperspectral TER map (Figure 3B). Note that the entire field of view in constantly irradiated with the laser (objective NA=0.7). Although modest contrast (~1.8x) is observed between on-particle (region 2) *vs* on-silicon spectra, the edge response is on average ~3.5x/6.4x brighter than the optical signal atop the particle/silicon.

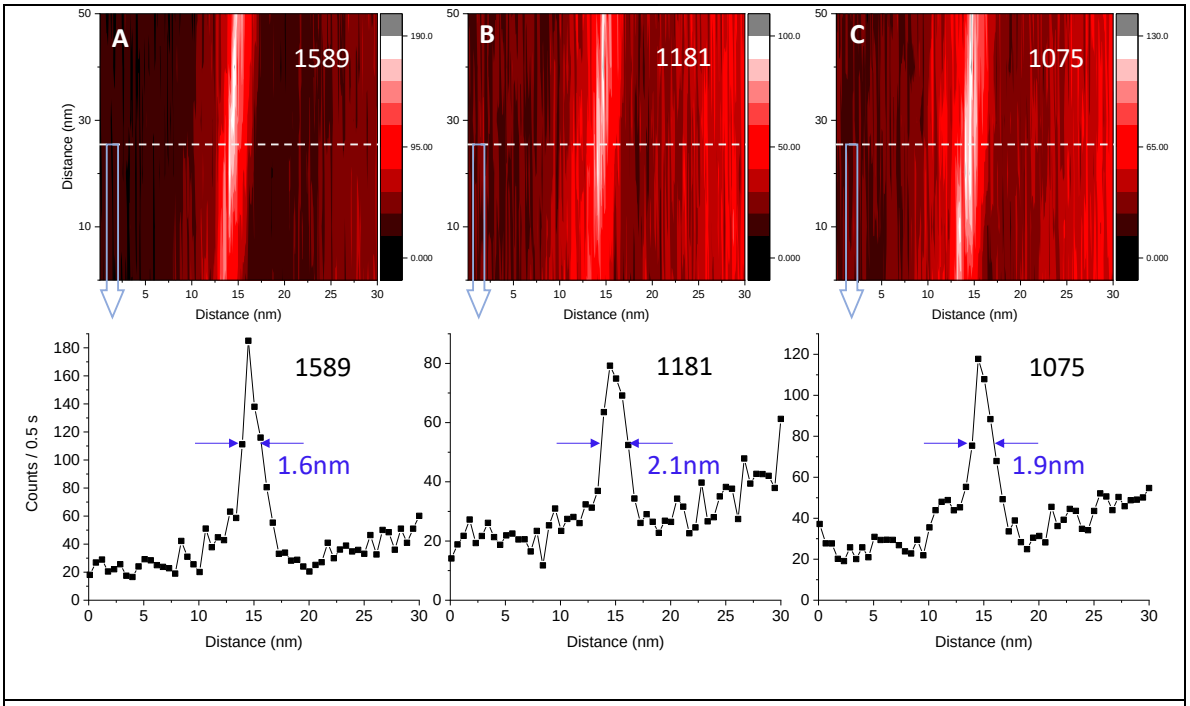

Figure 4. Spectrally-resolved TER nano-imaging of the cube at different resonances of the molecular reporter: 1589 cm^{-1} (A), 1181 cm^{-1} (B), and 1075 cm^{-1} (C). The lower panels in each case correspond to cuts taken at the positions indicated in the upper panels. Note that these images were simultaneously recorded with the image shown in Figure 3B (they belong to the same hyperspectral TER image cube). As such, the same imaging parameters were naturally used herein.

Spectrally-resolved TER maps at different vibrational resonances of TBN are shown in Figure 4. Images traced at different frequencies within our Stokes window are similar in overall

structure; they only vary in their overall signal magnitudes in a way that is more-or-less commensurate (more on this below) with the Raman activities of the different modes. This is contrasted with a recent report from our group,[20] whereby sharp multipolar resonances contained within the Stokes window were tracked through the recorded TER spectra and images. This observation indicates that the operative resonance in this case is broad and does not vary dramatically within the accessible wavelength range (640-740 nm). This finding is somewhat consistent with a recent theoretical analysis of hybrid tip-sample plasmonic nanojunctions in the TER geometry.[36] TER cuts across the edge of the particles at different frequencies otherwise reveal spatial resolutions that are comparable to their analogue in Figure 3C. More evidence in support of the results described thus far in Figures 3 and 4 are given in the supporting information section of this work.

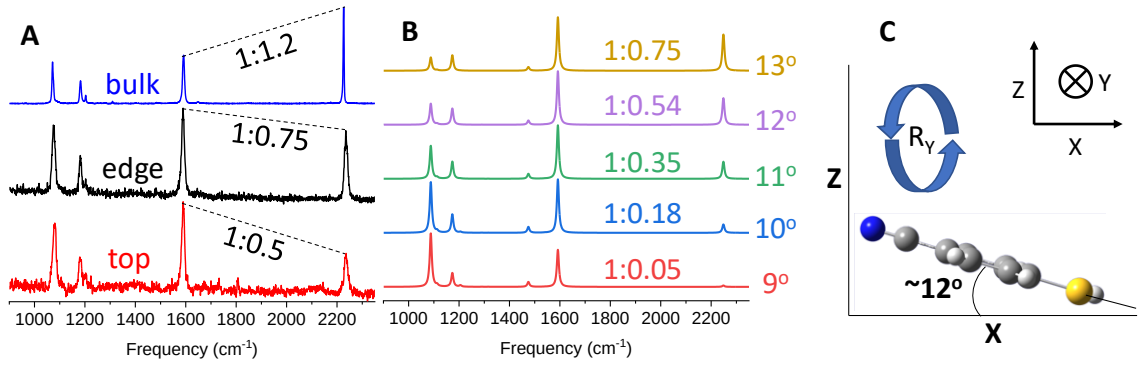

Figure 5. Panel A shows experimental spectra taken from Figure 2 (bulk) and Figure 3D (edge = region 1 and top = region 2, as highlighted in Figure 3B). The relative intensities of the 1589:2225 cm^{-1} bands are noted in the same panel. Panel B shows simulated single molecule Raman spectra obtained by rotating the molecule around the Y-axis (9-13°). The relative intensities of the 1589:2225 cm^{-1} bands are also shown in the inset of this panel. Panel C shows the laboratory frame and a schematic illustration of the molecule, which is rotated by 12° around its Y-axis. Note that the incident and scattered local field are $\overrightarrow{E^L_{i,s}} = \overrightarrow{E^L_z}$. See equation 4 and the main text for more details.

We can account for the observed differences in the relative intensities of the vibrational modes of TBN in the bulk (see Figure 2) and in the TER geometry (see Figure 3) by invoking the

formalism summarized by equation 4. Namely, given the attainable spatial resolution that is demonstrated in Figures 3 and 4, ensemble-averaging of the recorded optical response is no longer appropriate.[16, 32] The starting point for our analysis is to ensure that the ensemble-averaged spectra are well-reproduced at the level of theory used to compute the Raman spectra. Indeed, the results shown in Figure 2 confirm that the general features that are observed in bulk (TBN powder) experiments are well reproduced in the computed spectra, even though the bare molecule is used *in silico*. As mentioned in the methods sub-section of this manuscript, however, the agreement in terms of the relative intensities of the vibrational states is only optimal in the high frequency region of the spectrum, which contains the aromatic CC (1589 cm^{-1}) and CN (2225 cm^{-1}) stretching vibrations of TBN. We next model the dependence of the simulated spectra on molecular orientation with respect to vector components of the local optical fields ($\overrightarrow{E^L_{l,s}} = \overrightarrow{E^L_z}$ in the TER geometry).[10] Rather than performing full search in Euler space,[16, 32, 34] we guide our search using the orientation that was calculated from geometry optimization of the Ag_{79}-TBN complex (see Figure 1). The results are shown in Figure 5, where simulated molecular orientation-dependent Raman spectra are compared to experimental bulk and TER spectra. Experimentally, the intensities of the 1589 cm^{-1} relative to the 2225 cm^{-1} modes are very different in the bulk *vs* TER spectra (see Figure 5A). Although the former can be readily rationalized based on conventional orientationally averaged theoretical spectra (Figure 2), the latter requires considering molecular orientation. This is shown in Figure 5B, where we also illustrate that slight molecular rotations around the Y axis in the laboratory frame (defined in Figure 5C) yields noticeably different relative intensities of the 1589 *vs* 2225 cm^{-1} lines.

The best match between theory and the experimentally recorded TER spectra (both edge and atop the particle) is obtained when the molecule is rotated by ~12-13^o with respect to the Y-

axis (see Figure 5). This result is largely consistent with the computed orientation of TBN relative to Ag_{79} in the optimized Ag_{79}-TBN complex (see Figure 1). The derived geometry is however dissimilar from what can be inferred from (diffraction-limited)/ensemble averaged SER scattering from TBN on a polycrystalline silver surface, which we have recently analyzed using ensemble averaged/orientation-dependent Raman spectra derived from *ab initio* molecular dynamics simulations.[35] Namely, the orientation of TBN on a nominally flat surface is different from its orientation on the tip. This emphasizes that whereas the Ag_{79}-TBN complex seems to be representative of the tip-bound molecule, it is not representative of the most frequently sampled orientation on a nominally flat surface, as gauged through SER scattering. It also strongly suggests that a single molecule (or very few) governs the recorded optical response in high spatial resolution TER spectral imaging.

Conclusions

Overall, through a combination of high spatial resolution TER nano-imaging and nano-spectroscopy and density functional theory simulations, we describe a protocol that may be used to map 3D molecular orientation with ~2 nm nanometer lateral spatial resolution. As a result of the (nearly flat) molecular geometry in our current study and TER selection rules ($\overrightarrow{E^L_{i,s}} = \overrightarrow{E^L_z}$), we were able to pin-point the 3D orientation of a TBN molecule with high accuracy through simulations of tensorial Raman scattering that were guided by a geometry optimization of a Ag_{79}-TBN complex. The derived orientation is different from the most frequently sampled geometry of TBN on nominally flat Ag, as previously gauged through SERS. It is thus tempting to associate the spectra with a single molecule (or at most a few). Unlike existing frequency

domain proofs of single molecule detection sensitivity,[37] our demonstration of ~2 nm spatial resolution in the same measurements used to infer 3D molecular orientation strongly supports our claim of single molecule detection sensitivity (or at most a few). Nonetheless, looking forward, it would be interesting to combine the protocol described herein with previously described robust approaches to ascertaining single molecule sensitivity in the frequency domain.[37] Such measurements are currently underway in our laboratory.

AUTHOR INFORMATION

Corresponding Author

*patrick.elkhoury@pnnl.gov

The authors declare no competing financial interest.

ACKNOWLEDGMENTS

This work was supported by the US Department of Energy (DOE), Office of Science, Office of Basic Energy Sciences, Division of Chemical Sciences, Geosciences & Biosciences. A portion of the research was performed at EMSL, a DOE Office of Science User Facility sponsored by the office of biological and environmental research (BER) and located at Pacific Northwest National Laboratory (PNNL). PNNL is operated by Battelle Memorial Institute for the United States Department of Energy under DOE contract number DE-AC05-76RL1830. The authors are grateful to Niranjan Govind (PNNL) for useful discussions.

SUPPORTING INFORMATION

TER measurements performed using a different AFM probe, and which show similar spatial resolution compared to the results shown in the main text; optimized coordinates of the Ag_{79}-TBN complex.

TOC Graphic

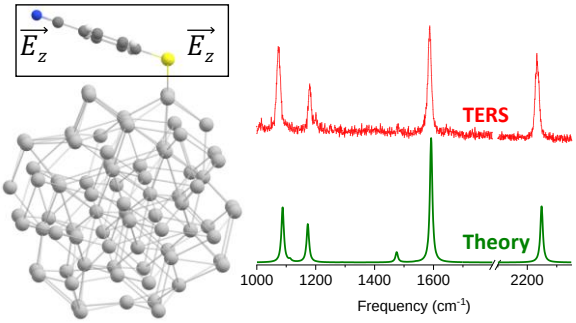
$\overrightarrow{E_z}$
$\overrightarrow{E_z}$
TERS
Theory
1000
1200
1400
1600
2200
Frequency (cm-1)

References

1. Anderson, M. S. *Locally Enhanced Raman Spectroscopy with an Atomic Force Microscope*. *Appl. Phys. Lett.* **2000**, *76*, 3130-3132.
2. Stockle, R. M.; Suh, Y. D.; Deckert, V.; Zenobi, R. *Nanoscale Chemical Analysis by Tip-Enhanced Raman Spectroscopy*. *Chem. Phys. Lett.* **2000**, *318*, 131-136.
3. Pettinger, B.; Schambach, P.; Villagómez, C. J.; Scott, N. *Tip-Enhanced Raman Spectroscopy: Near-Fields Acting on a Few Molecules*. *Annu. Rev. Phys. Chem.* **2012**, *63*, 379-399.
4. Fleischmann, M.; Hendra, P. J.; Mcquilla, A. J. *Raman-Spectra of Pyridine Adsorbed at a Silver Electrode*. *Chem. Phys. Lett.* **1974**, *26*, 163-166.
5. Jeanmaire, D. L.; Vanduyne, R. P. *Surface Raman Spectroelectrochemistry .1. Heterocyclic, Aromatic, and Aliphatic-Amines Adsorbed on Anodized Silver Electrode*. *J. Electroanal. Chem.* **1977**, *84*, 1-20.
6. Moskovits, M. *Surface-Roughness and Enhanced Intensity of Raman-Scattering by Molecules Adsorbed on Metals*. *J. Chem. Phys.* **1978**, *69*, 4159.
7. Otto, A. *Raman-Spectra of CN^- Adsorbed at a Silver Surface*. *Surf. Sci.* **1978**, *75*, L392-L396.
8. He, Z.; Han, Z. H.; Kizer, M.; Linhardt, R. J.; Wang, X.; Sinyukov, A. M.; Wang, J. Z.; Deckert, V.; Sokolov, A. V.; Hu, J.; Scully, M. O. *Tip-Enhanced Raman Imaging of Single-Stranded DNA with Single Base Resolution*. *J. Am. Chem. Soc.* **2019**, *141*, 753-757.
9. Zhang, R.; Zhang, Y.; Dong, Z. C.; Jiang, S.; Zhang, C.; Chen, L. G.; Zhang, L.; Liao, Y.; Aizpurua, J.; Luo, Y.; Yang, J. L.; Hou, J. G. *Chemical mapping of a single molecule by plasmon-enhanced Raman scattering*. *Nature* **2013**, *498*, 82-86.
10. Lee, J.; Crampton, K. T.; Tallarida, N.; Apkarian, V. A. *Visualizing vibrational normal modes of a single molecule with atomically confined light*. *Nature* **2019**, *568*, 78-82.
11. Pozzi, E. K.; Goubert, G.; Chiang, N. H.; Jiang, N.; Chapman, C. T.; McAnally, M. O.; Henry, A. I.; Seideman, T.; Schatz, G. C.; Hersam, M. C.; Van Duyne, R. P. *Ultrahigh-Vacuum Tip-Enhanced Raman Spectroscopy*. *Chem. Rev.* **2017**, *117*, 4961-4982.
12. Richard-Lacroix, M.; Zhang, Y.; Dong, Z. C.; Deckert, V. *Mastering High Resolution Tip-Enhanced Raman Spectroscopy: Towards a Shift of Perception*. *Chem. Soc. Rev.* **2017**, *46*, 3922-3944.
13. Wang, C. F.; O'Callahan, B. T.; Kurouski, D.; Krayev, A.; El-Khoury, P. Z. *The Prevalence of Anions at Plasmonic Nanojunctions: A Closer Look at p-Nitrothiophenol*. *J. Phys. Chem. Lett.* **2020**, 3809-3814.
14. Bhattarai, A.; Novikova, I. V.; El-Khoury, P. Z. *Tip-Enhanced Raman Nanographs of Plasmonic Silver Nanoparticles*. *J. Phys. Chem. C* **2019**, *123*, 27765-27769.
15. Bhattarai, A.; Crampton, K. T.; Joly, A. G.; Kovarik, L.; Hess, W. P.; El-Khoury, P. Z. *Imaging the Optical Fields of Functionalized Silver Nanowires through Molecular TERS*. *J. Phys. Chem. Lett.* **2018**, *9*, 7105-7109.
16. Bhattarai, A.; Joly, A. G.; Hess, W. P.; El-Khoury, P. Z. *Visualizing Electric Fields at Au(111) Step Edges via Tip-Enhanced Raman Scattering*. *Nano Lett.* **2017**, *17*, 7131-7137.
17. Bhattarai, A.; El-Khoury, P. Z. *Imaging localized electric fields with nanometer precision through tip-enhanced Raman scattering*. *Chem. Commun.* **2017**, *53*, 7310-7313.
18. Bhattarai, A.; Cheng, Z.; Joly, A. G.; Novikova, I. V.; Evans, J. E.; Schultz, Z. D.; Jones, M. R.; El-Khoury, P. Z. *Tip-Enhanced Raman Nanospectroscopy of Smooth Spherical Gold Nanoparticles*. *J. Phys. Chem. Lett.* **2020**, *11*, 1795-1801.
19. Bhattarai, A.; Joly, A. G.; Krayev, A.; El-Khoury, P. Z. *Taking the Plunge: Nanoscale Chemical Imaging of Functionalized Gold Triangles in H2O via TERS*. *J. Phys. Chem. C* **2019**, *123*, 7376-7380.
20. Bhattarai, A.; O'Callahan, B. T.; Wang, C. F.; Wang, S.; El-Khoury, P. Z. *Spatio-Spectral Characterization of Multipolar Plasmonic Modes of Au Nanorods via Tip-Enhanced Raman Scattering*. *J. Phys. Chem. Lett.* **2020**, *11*, 2870-2874.

21. Bhattarai, A.; El-Khoury, P. Z. *Nanoscale Chemical Reaction Imaging at the Solid–Liquid Interface via TERS*. *J. Phys. Chem. Lett.* **2019**, 2817-2822.
22. Bhattarai, A.; Crampton, K. T.; Joly, A. G.; Wang, C. F.; Schultz, Z. D.; El-Khoury, P. Z. *A Closer Look at Corrugated Au Tips*. *J. Phys. Chem. Lett.* **2020**, *11*, 1915-1920.
23. Sun, J. J.; Su, H. S.; Yue, H. L.; Huang, S. C.; Huang, T. X.; Hu, S.; Sartin, M. M.; Cheng, J.; Ren, B. *Role of Adsorption Orientation in Surface Plasmon-Driven Coupling Reactions Studied by Tip-Enhanced Raman Spectroscopy*. *J. Phys. Chem. Lett.* **2019**, *10*, 2306-2312.
24. Aprà, E. et al. *NWChem: Past, Present, and Future. J. Chem. Phys.* **2020**, *152*, 184102.
25. Perdew, J. P.; Burke, K.; Ernzerhof, M. *Generalized gradient approximation made simple*. *Phys. Rev. Lett.* **1996**, *77*, 3865-3868.
26. Weigend, F.; Ahlrichs, R. *Balanced basis sets of split valence, triple zeta valence and quadruple zeta valence quality for H to Rn: Design and assessment of accuracy*. *Phys. Chem. Chem. Phys.* **2005**, *7*, 3297-3305.
27. Weigend, F. *Accurate Coulomb-fitting basis sets for H to Rn*. *Phys. Chem. Chem. Phys.* **2006**, *8*, 1057-1065.
28. Grimme, S.; Antony, J.; Ehrlich, S.; Krieg, H. *A consistent and accurate ab initio parametrization of density functional dispersion correction (DFT-D) for the 94 elements H-Pu*. *J. Chem. Phys.* **2010**, *132*, 154104.
29. Kellö, V.; Sadlej, A. J. *Medium-size polarized basis sets for high-level-correlated calculations of molecular electric properties*. *Theor. Chim. Acta* **1992**, *83*, 351-366.
30. Cardona, M.; Guntherodt, G. *Light-Scattering in Solids .2. Basic Concepts and Instrumentation - Introduction*. *Top. Appl. Phys.* **1982**, *50*, 1-18.
31. Murphy, W. F.; Holzer, W.; Bernstein, H. J. *Gas Phase Raman Intensities - a Review of Pre-Laser Data*. *Appl. Spectrosc.* **1969**, *23*, 211.
32. Banik, M.; El-Khoury, P. Z.; Nag, A.; Rodriguez-Perez, A.; Guarrottxena, N.; Bazan, G. C.; Apkarian, V. A. *Surface-Enhanced Raman Trajectories on a Nano-Dumbbell: Transition from Field to Charge Transfer Plasmons as the Spheres Fuse*. *ACS Nano* **2012**, *6*, 10343-10354.
33. Wang, C. F.; Cheng, Z.; O'Callahan, B. T.; Crampton, K. T.; Jones, M. R.; El-Khoury, P. Z. *Tip-Enhanced Multipolar Raman Scattering*. *J. Phys. Chem. Lett.* **2020**, 2464-2469.
34. Apra, E.; Bhattarai, A.; Crampton, K. T.; Bylaska, E. J.; Govind, N.; Hess, W. P.; El-Khoury, P. Z. *Time Domain Simulations of Single Molecule Raman Scattering*. *J Phys. Chem. A* **2018**, *122*, 7437-7442.
35. Apra, E.; Bhattarai, A.; El-Khoury, P. Z. *Gauging Molecular Orientation through Time Domain Simulations of Surface-Enhanced Raman Scattering*. *J. Phys. Chem. A* **2019**, *123*, 7142-7147.
36. Yang, M.; Mattei, M. S.; Cherqui, C. R.; Chen, X.; Van Duyne, R. P.; Schatz, G. C. *Tip-Enhanced Raman Excitation Spectroscopy (TERES): Direct Spectral Characterization of the Gap-Mode Plasmon*. *Nano Lett.* **2019**, *19*, 7309-7316.
37. Zrimsek, A. B.; Wong, N. L.; Van Duyne, R. P. *Single Molecule Surface-Enhanced Raman Spectroscopy: A Critical Analysis of the Bianalyte versus Isotopologue Proof*. *J. Phys. Chem. C* **2016**, *120*, 5133-5142.